Small pixel pitch MCT P on N MWIR photodiodes at DEFIR: towards 7.5um and beyond with very high image quality

Nicolas Baier, Olivier Gravrand, Titouan Legoff, Clément Lobre, Florent Rochette, Alexandre Brunner, Cécile Grezes, Nicolas Morisset, Laurent Rubaldo

PROCEEDINGS OF SPIE

SPIEDigitalLibrary.org/conference-proceedings-of-spie

Small pixel pitch MCT P on N MWIR photodiodes at DEFIR: towards 7.5um and beyond with very high image quality

N. Baier, O. Gravrand, T. Le Goff, C. Lobre, W. Rabaud, et al.

N. Baier, O. Gravrand, T. Le Goff, C. Lobre, W. Rabaud, F. Rochette, A. Brunner, C. Grezes, N. Morisset, L. Rubaldo, "Small pixel pitch MCT P on N MWIR photodiodes at DEFIR: towards 7.5um and beyond with very high image quality," Proc. SPIE 12534, Infrared Technology and Applications XLIX, 1253413 (13 June 2023); doi: 10.1117/12.2663760

SPIE.

Event: SPIE Defense + Commercial Sensing, 2023, Orlando, Florida, United States

Small pixel pitch MCT P on N MWIR photodiodes at DEFIR: towards 7.5µm and beyond with very high image quality

N. Baier[a*], O. Gravrand[a], T. Le Goff[a], C. Lobre[a], W. Rabaud[a], F. Rochette[a], A. Brunner[b], C. Grezes[b], N. Morisset[b], L. Rubaldo[b]

*nicolas.baier@cea.fr

[a]Univ. Grenoble Alpes, CEA, LETI – 17 Avenue des Martyrs, 38000 Grenoble (France)
[b]LYNRED, BP21, 38113 Veurey-Voroize, France

ABSTRACT

MCT p-on-n photodiodes manufactured at Lynred and CEA-LETI have demonstrated state of the art performances for HOT applications. On blue and red mid infrared bands on 15µm pixel pitch, respectively 150 and 130K operating temperatures have been obtained, due to diffusion limited dark current and low defectivity. To achieve equivalent results on smaller pixel, the p-on-n technology at DEFIR, joint laboratory between Lynred and CEA-LETI, has been improved. The technological process was modified to ensure a proper diode formation and to efficiently passivate the interface between MCT and encapsulation layers, especially in the vicinity of the space charge region. The manufactured arrays with a 5.3µm cutoff wavelength have been hybridized on a digital output SXGA (1280×1024) direct injection ROIC with a pixel pitch of 7.5 µm. This paper present the measured current, blackbody responsivity and RMS noise on FPAs with F/4 numerical aperture. We will also discuss spectral response, quantum efficiency, shot-noise limited photodiodes and noise histograms shapes and their distribution tails at 130K. The very low number of defective pixel allow to address higher operating temperature and measurements have been performed at 140K and even 150K with very limited performance degradation. Pixel pitch of 5 µm has been characterized on test chips and present I-V curves with low dispersion and long bias plateau. As for larger pixel sizes, these photodiodes are shot-noise limited. Modulation transfer function has been measured by electron beam induced current and presents high value, up to 56%.

Keywords: MCT, p/n, FPA, HOT, small pixel pitch, MWIR, RTN, MTF.

1. INTRODUCTION

P-on-n HgCdTe technology developments at DEFIR, the joint laboratory between Lynred and CEA-LETI, have started in 2009 [1] with the first array presented in 2010 [2]. This technology has been introduced at that time to address high operating temperature (HOT) challenges. The standard technology, based on mercury vacancies doping (VHg), presents indeed a higher dark current, limiting its capabilities to operate at a temperature higher than 110K for a mid-wavelength infrared detector (MWIR, 3 to 5 µm spectral band).

Many evolutions of the technology have been performed since those first achievements, for different purposes: performances enhancement to lower 1/f noise contribution, reduction of defective pixels for HOT applications in mid and long wavelength [3][4], short [5][6][7] and very long wavelength [8][9] array manufacturing for space applications. This technology has demonstrated all its capabilities to address many different applications.

However, all of the performances measured have been obtained on 15 µm pixel pitch photodiodes and readout integrated circuit (ROIC). To answer the needs of infrared systems ranges (detection, recognition or identification), minimum resolvable temperature difference (MRTD) and the associated modulated transfer function (MTF) have to be improved. Smaller pixel pitches are the key to meet the requirements [10]. Previous works have been presented by CEA-LETI on n-on-p diode technology with 10, 7.5 and 5 µm pixel pitch [11][12] and more recently on p-on-n technology [13] with superpixels made of 4 7.5 µm pitch diodes.

Infrared Technology and Applications XLIX, edited by Gabor F. Fulop, David Z. Ting, Lucy L. Zheng, Proc. of SPIE Vol. 12534, 1253413 · © 2023 SPIE
0277-786X · doi: 10.1117/12.2663760

This achievement was possible with the instruction of a new generation (NG) of p-on-n diode technology, developed by CEA-LETI and Lynred, which improves both manufacturability and noise performances.

2. TECHNOLOGY DESCRIPTION

The CdHgTe (MCT) absorbing layer is grown by liquid phase epitaxy on a latticed matched 47×48 mm² CdZnTe (CZT) substrate manufactured at CEA-LETI. These choices ensure an optimal material quality. Indium doping of the absorbing layer is done in-situ in the MCT melt, to get a doping in the range 1e15 to 1e16 cm^{-3}. P-on-n junction is formed by implanting As and then baked in the proper conditions to get a good diffusion and activation of the As. Finally, the layer obtained is passivated to protect the surface and to minimize the contribution of interface defects on performances. As can be seen, this NG technology seems to be very similar to the classical p-on-n planar photodiode presented in previous papers. However, this technology is more suitable to the manufacturing of small pixel pitch and appears to present better performances in terms of pixel defectivity.

3. CHARACTERIZED ARRAYS AND PROTOCOLS

3.1 ROIC description

Two types of arrays have been characterized. The first one is a classical VGA format 15 µm pixel pitch array with a direct injection input stage ROIC pixel and an analogic output. The capacitance is 780fF as the ROIC was designed for both mid and long wavelength infrared detectors (in MWIR range such a capacitance implies to use longer integration time). On this ROIC, the active layer is composed of 4 diodes coupled at the metallization level to obtain a superpixel connected to the ROIC pixel. Although an easy-to-go manufacturing and characterization on a well-known ROIC, the analysis of the performances of such an array suffers from the averaging of the performances (current and noise) of 4 diodes. This feature may mask some defective diodes.

The second ROIC is a SXGA format array with 7.5 µm pixel pitch, adapted to each photodiode of the detection array. It comes also with direct injection input stage pixel and an analog to digital conversion in the ROIC. The capacitance is adjustable through different gains and nominally set to 92fF. The digital output is a parallel 14 bits at high rate to ensure a high frame rate (up to 100Hz). This ROIC is a perfect tool to evaluate the diodes performances with a large statistic.

3.2 Arrays tested: diode variants exploration and measurement conditions

Hybridized focal plane arrays are divided in two groups. For the first one, the array is subdivided in multiple zones addressing different diodes flavor. Each flavor is a variation of the diode geometric parameters. The major advantage of such a device is to study the impact of one particular dimension on the performances of the diodes, within a single characterization run. The number of diode flavor depends on the ROIC: for VGA FPAs, 16 zones are materialized to study 8 different diodes variants (2 zones per diode type for redundancy purpose). For SXGA FPAs, we have 2 kinds of array, one with 4 zones of 2 diodes variants and one with 12 diode flavors (no redundancy in this case). The second group of arrays is for standard array with only one diode flavor on the array. Three or four flavors array are chosen amongst the available variants introduced previously and suspected to present the best behavior. With both of array types, we can estimate the major effect of each geometry parameter and measure with a large statistics the performances of the best ones.

Measurements have been performed on both type of detectors at 110 and 130K and for the best arrays also at 140 and 150K. Numerical aperture was F/4, with blackbody temperature of 20 and 35°C. I-V characteristics have been measured, leading to choose 2 to 4 biases for fine characterization of arrays properties: current, blackbody responsivity, quantum efficiency, RMS noise, noise equivalent temperature difference (NETD) and proportion of defects with random telegraph noise (RTN).

4. TEST-CHIP AND 7.5µm SXGA ARRAY PERFORMANCES

4.1 Spectral response

Test-chip consists of few tens of photodiodes that can be individually monitored. Each of these diodes are surrounded by other diodes, connected all together to reproduce the behavior of an array. With these kind of design we are able to compare measurements on test-chips and arrays. Test-chip diodes are measured to assess basic detection properties. Figure 1 present the spectral response measured with a Fourier Transform Infrared spectrometer (FTIR), on nine diodes from two test-chip of two different layers. The noise at short wavelength is due to the reference detector, which present a low efficiency, the

baseline correction thus introduce intense variation of the response. The cutoff wavelength, obtained at half maximum is around 5.1 ± 0.5 µm. The quasi-triangular shape of the response (in unit homogeneous to A/W) indicates a constant quantum efficiency (QE) on a large wavelength range. The QE value will be discussed later in the present paper.

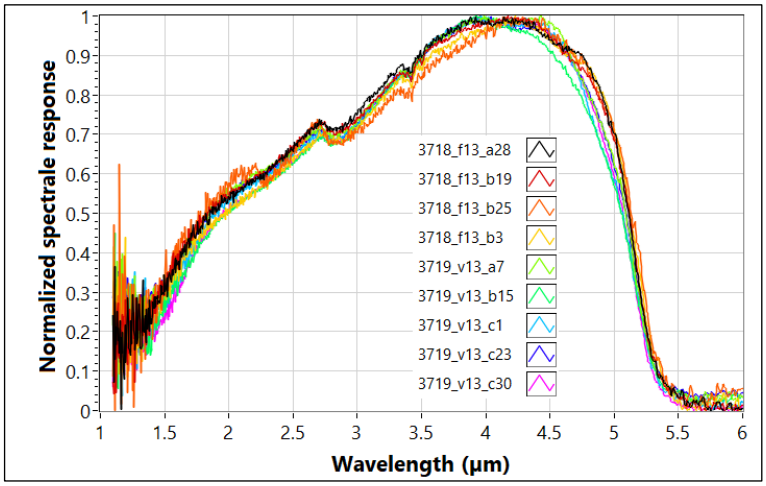

Figure 1. Normalized spectral response of 7.5 µm pitch diodes at 130K.

4.2 Photonic current and responsivity

SXGA array are characterized in front of a blackbody to determine both diode current and responsivity. For these measurements, integration time was set to 5ms. The gate bias of the injection MOS transistor is tuned to obtain an I-V curve for each diode. A statistical analysis is then performed to get the mean current and the number of pixels in the operating range (defined as ±50% of mean value). The results are presented in Figure 2. The gate bias varies from 0.68 to 2.79V, the threshold voltage of the MOS transistor (typically 0.65V) has to be subtracted to these values to determine the effective diodes bias (thus ranging from few tenth of mV to more than 2V). The numerical aperture is F/3.

The photonic current is equal to 7.72pA at low bias and increases slightly with bias (less than 2% over 2V). The bias plateau is very large, greater than 1V. Dynamic resistance varies from 200TΩ (maximum at low bias) to 5TΩ at higher bias, with diodes starting to present a very small contribution of leakage current. In the same time, we can notice that the operability (fraction of properly operating pixels) is very high, above 99.9% with a loss of only 0.03 points in the studied range. The operability degradation results from a small amount of pixels presenting leakage current at lower bias than the rest of the array.

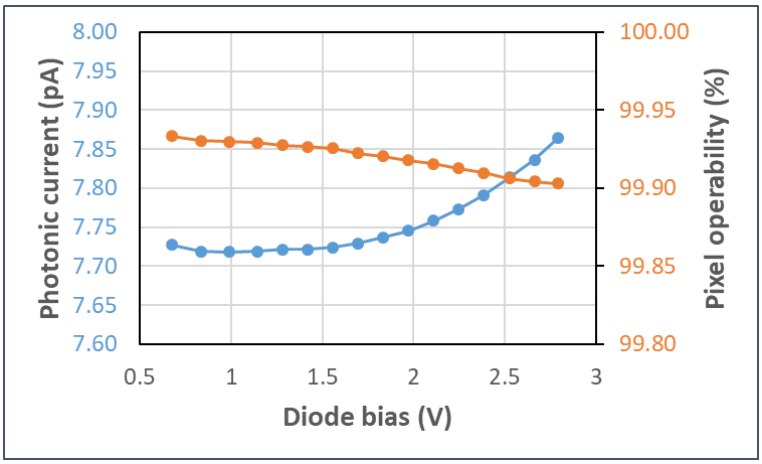

Figure 2. SXGA mean current (35°C blackbody) and corresponding pixel operability (±50% of mean value) at 130K.

With this current-bias characteristic, we can determinate the nominal bias to apply to the detector to get the best performances. A bias of 0.75V on the injection MOS gate ensures the best compromise between high resistance, low dispersion and high operability. The current obtained is presented on Figure 3, with its mapping over the array and its steep histogram. Mean current is 10.85pA with an operability of 99.91% (1140 defective pixels for 1.3M pixels array) and an overall dispersion of 2.6%. Responsivity to blackbody is 0.49pA/K on this array, with the same figures for operability and dispersion.

Using the spectral response presented previously, the responsivity measurements and with a proper radiometric calculation (knowing all the optical parameters of the setup) we could estimate the quantum efficiency of the arrays of 85±5%. This result is in good agreement with measurements performed at Lynred on a different test bench, using a cold pass band filter [3.7µm, 4.8µm] [14].

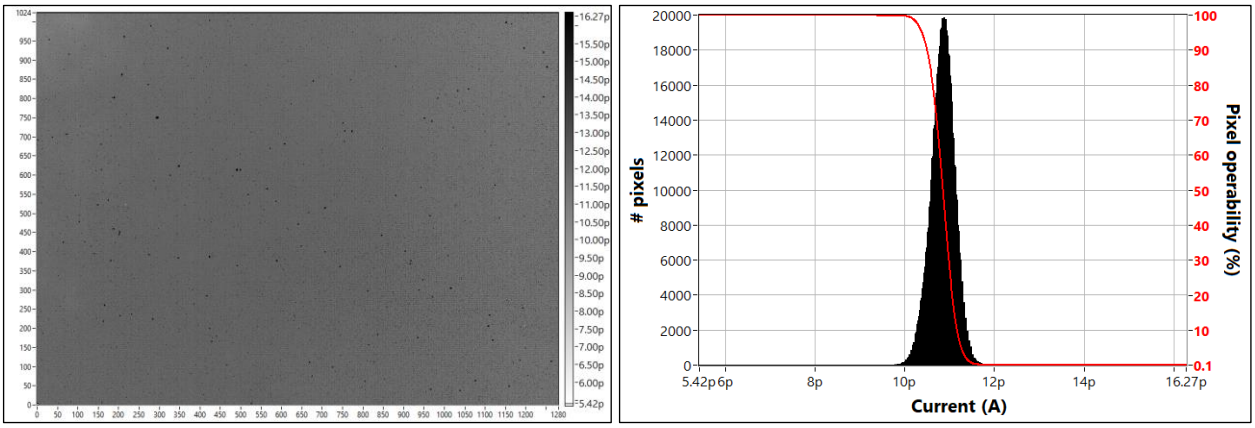

Figure 3. SXGA current mapping and corresponding histogram for 20°C blackbody temperature, 5ms integration time, at 130K.

5. NOISE MEASUREMENTS: A BREAKTHROUGH IN PIXEL DEFECTIVITY

5.1 Noise distribution and defects

In a previous work [13], the very first RMS noise measurement on 4 quadrant SXGA array have been presented. One specific diode design exhibits RMS noise operability of 99.99% at 130K, while the other variant suffer a degradation between 110 and 130K. The technology has been improved since, to converge to both a manufacturing process and a diode geometry that fulfills our goals to lower at best the pixel defectivity. The noise measurements presented hereafter are corrected from the ROIC and acquisition setup noise, to evaluate the diodes themselves. We are able to directly compare this noise to the theoretical shot-noise of a photodiode given by $\sqrt{2qI_{ph}}$, where I_{ph} is the photonic current of the diode. For every array tested, the ratio between the corrected noise and the shot-noise is very close to 1, highlighting that there is no other contribution to the noise than the photonic one.

In the latest batches, 12-quadrant SXGA arrays have been characterized to evaluate the different new designs introduced. Some of the variants have particularly high operability while other one still present a low distribution tail at 130K. Figure 4 presents the histograms of 4 diode flavors on 109k pixel areas at 130K. A first indicator giving the main geometry design and a second one concerning second order parameters compose the label describing each variant. It appears that 2 variants have an excellent behavior without any distribution tail and an operability of 99.99% (less than 15 defective pixels with a ±100% mean value criterion). For the two other ones, operability suffers a 0.26 point operability decrease between 110 and 130K.

The best variant have been implemented on a full SXGA array to verify we get the same performances on a larger scale. As can be seen on Figure 5, we obtained a very good result, with a Gaussian distribution, a very low tail at 130K and an operability of 99.97% (with a ±100% mean value criterion), less than 370 defective pixels on the entire array. This result highlights the impressive capabilities of this p-on-n NG technology at DEFIR on small pixel pitch and large format array, as we can discriminate defective pixels one by one on the distribution.

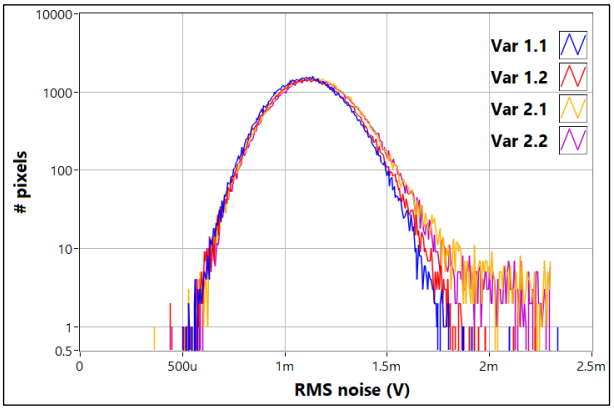

Figure 4. RMS noise distribution of 4 areas of a 12-quadrant SXGA array, for 27°C blackbody temperature at 130K.

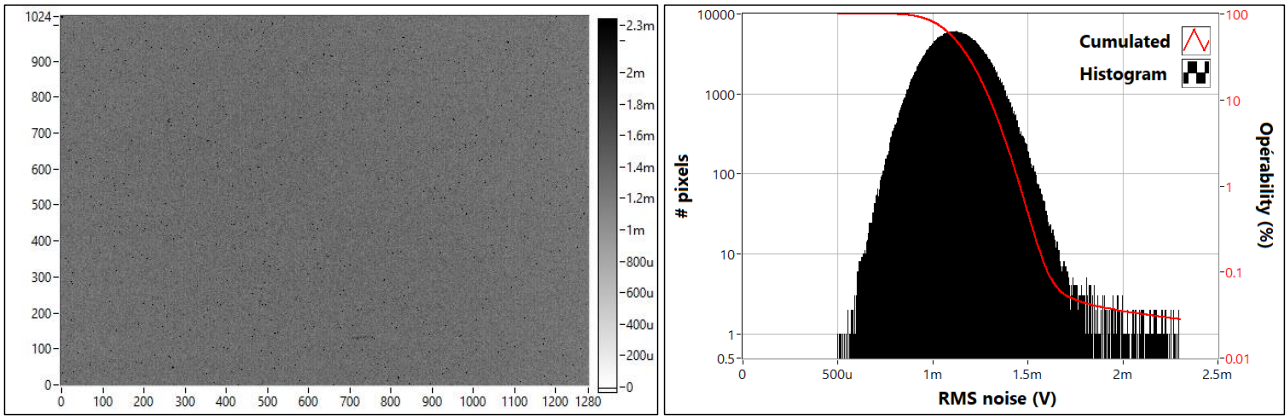

Figure 5. RMS noise mapping and distribution on a full SXGA array, for 27°C blackbody temperature at 130K.

5.2 Effect of operating temperature

On a superpixel VGA format array, we went even further to evaluate the performances at higher temperature. In the same conditions (F/4 numerical aperture, 25°C blackbody temperature and nominal bias) we rose the detector temperature to 130, 140 and 150K. On the same type of variant as used in the arrays presented above, we found that the noise distribution have the same shape at the 3 temperatures, as can be seen on Figure 6. No tail appears while increasing the operating temperature, only the flank of the distributions are a bit softer than a pure normal distribution. The distributions are gradually shifted to lower noise values, as a result of MCT bandgap increase [15]. Therefore, the photonic current and its associated noise decrease with the temperature, however the measured noise is still limited by shot-noise.

The respective operabilities are 99.97%, 99.98% and 99.95% corresponding to 6, 4 and 10 defective pixels on a 20.5k pixel ($1/16^{th}$ of the array). This very promising result has yet to be confirmed on a SXGA format array with the same diode flavor.

5.3 RTN contribution to defective pixels

Noise analysis presented previously are typically performed with a measurement of 200 images at nominal frame rate (25 to 30Hz depending on the integration time in an integration then read mode). Such an image acquisition lasts only a few seconds and thus is not sufficient to detect properly pixel with random telegraph noise (RTN) [16]. RTN pixels present broad distributions in terms of amplitude and especially in transition times between states [17]. It is mandatory to have a long time measurements to observe rare RTN transition, which may concern an important fraction of pixels with RTN behavior. The characterization setup used here allows acquiring 10k images at 4 to 5Hz frame rate, corresponding to more than half an hour of pixel observation.

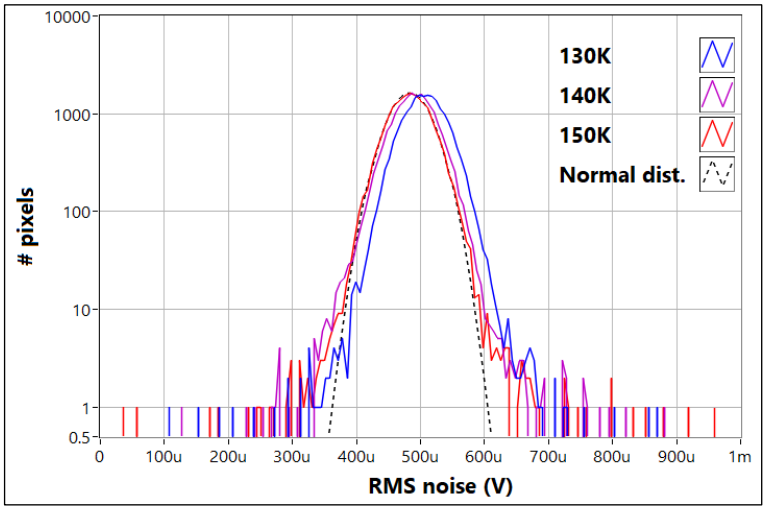

Figure 6. RMS noise distribution of one variant of a 16-quadrant VGA array, at 130K, 140K and 150K.

Such a measurement have been performed on a VGA format, superpixel array at 130K. Once again, the studied detector is a 16-quadrant array. Figure 7 present a comparison between RMS noise and RTN defective pixels at 130K for 3 variants of the array. We can see that there is a strong correlation between the number of RMS noise and RTN defective pixels, with less RTN ones. This results highlights that RTN is not the main defectivity contributor and with the proper technology tuning and design choice we can decrease both defective pixels (excess RMS noise and RTN).

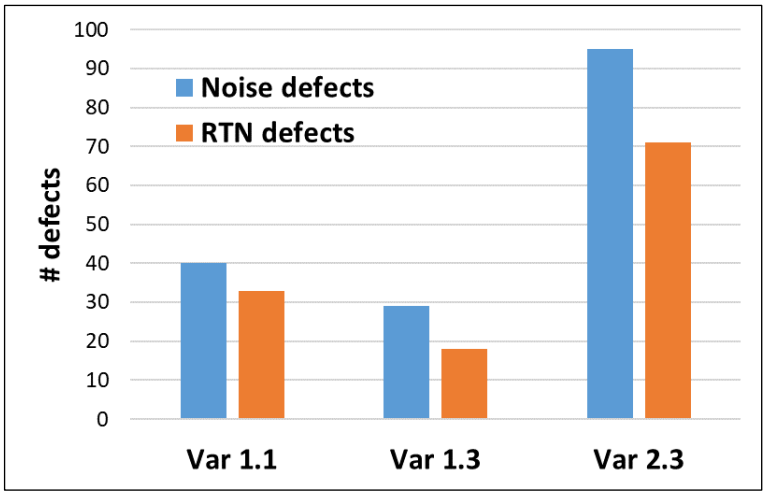

Figure 7. Number of defective pixels on a standard noise measurement and a specific RTS detection measurement at 130K on a 16-quadrant VGA format array.

One key point to notice about the two defective pixel population concerns their respective overlapping. Since the observation time domains are dramatically different (few seconds at high frame rate versus half an hour at low frame rate) there are portions of pixels that are detected only in one measurement. Finally, to compare these values with RMS noise measurement presented above, the operability is going from 99.88% (noise defects on variant 2.3) to 99.97% (RTN defects on variant 1.3).

It is also interesting to study the behavior of the RTN pixels population with operating temperature. We have observed previously that on the best variant, the number of RMS noise defects tend to stay relatively constant as we increase the temperature. Figure 8 presents the progressive evolution of RTN defects when the temperature is raised from 130K to 140K and further to 150K, for 4 variants. The FPA studied here is different from the previous one, the diodes do not have the same exact design nor technology process and therefore we focused the analysis on the main design contributor.

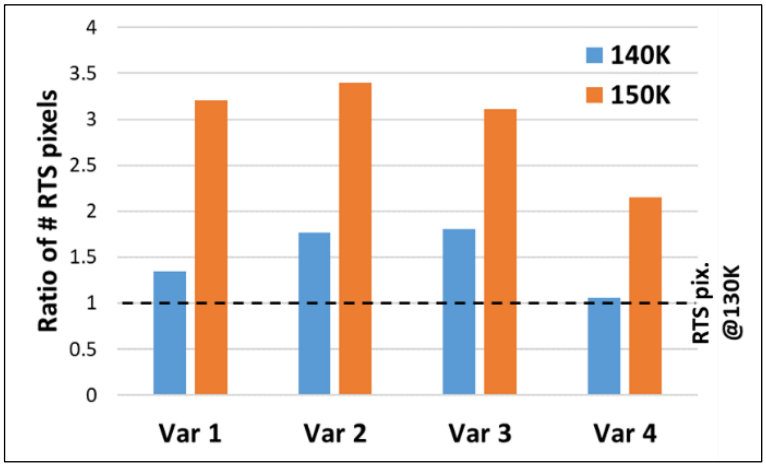

Figure 8. Ratio of defective RTS type pixels between 130K and 140K (blue) and 150K (orange) on a 16-quadrant VGA format array.

All variants suffer an increase of pixels with RTN, but the intensity differs. While it seems contained for variants 1 and 4, for variant 3 there are nearly twice more pixels. At 150K, it is unfortunately worse, the number of RTN pixels is tripled, except for variant 4 which exhibits a better behavior, with only twice more defects. Once again, this result highlights the fact that it is mandatory to select carefully design and technology to obtain the best performance on this p-on-n NG technology.

6. BEYOND 7.5µM PITCH, 1ST PERFORMANCES OF 5µm TEST CHIPS

Very promising results have been obtained on 7.5 µm pixel pitch test-chips and FPAs, in terms of quantum efficiency, defective pixels, MTF and dark current, discussed in the present paper and other studies [14][18][19]. We decided to evaluate the p-on-n NG technology at DEFIR at even smaller pixels. 5 µm pixel pitch diodes have been designed, inspired by the design of the 7.5 µm diodes with the best performances.

Measurement were performed on test-chip as no ROIC is available now with a compatible pixel pitch. Figure 9 present current-bias characteristics of various pixel pitch diodes. Each set of curves is composed of 50 diodes randomly selected at wafer level. The pitch ranges from 15 to 5 µm under front side illumination with IR LED on a tip test bench (at wafer level) and at 130K. We can observe they all have the same behavior; only the measured current is lower as the pitch decreases (same current density but smaller detection area). There shunt resistances vary from 500 MΩ (15µm pitch) to 5 GΩ (5µm pitch). The bias plateau, before the current increase due to tunneling effect at high bias, is around 3V and is larger for smaller pitches. This result is particularly promising to manufacture large arrays of very small pixel pitch, or for superpixel arrays that will present very few defects due to the averaging effect.

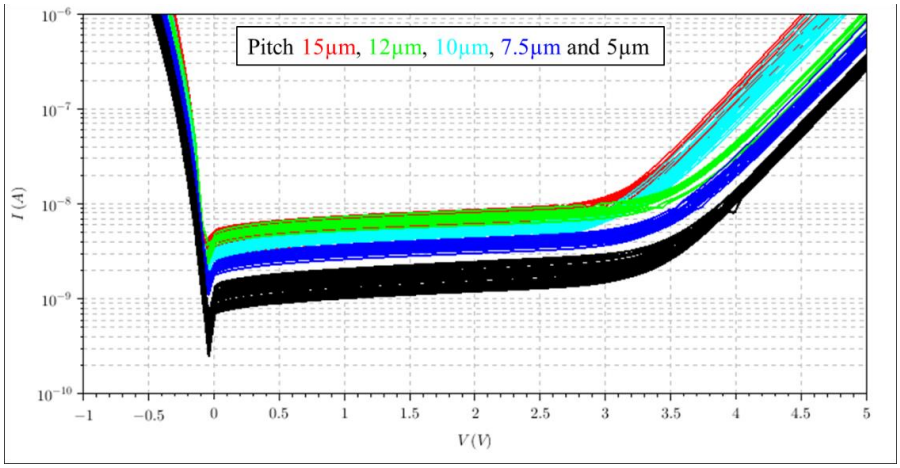

Figure 9. Current-bias characteristics for groups of diodes of different pixel pitch, measured on test chip at 130K.

To verify that detectors based on these diodes will meet the requirements of infrared imaging systems, naming MRTD, we measured the MTF of 7.5 and 5 µm. This measurement is performed by electron beam induced current (EBIC) in a second electron microscope (SEM). With a sharp spot, it allows a very precise measurement of pixel point spread function (PSF) which is transformed with a Fourier transformation to obtain the MTF [20][21]. Different kind of pixels have been studied and the results are presented on Figure 10. We can observe that for properly designed pixels, the MTF can reach very high values, up to 56% and 50% respectively for 7.5 µm and 5 µm pitch, to be compared to ideal value of 64% at Nyquist frequency. These results are discussed more precisely in a specific paper [18].

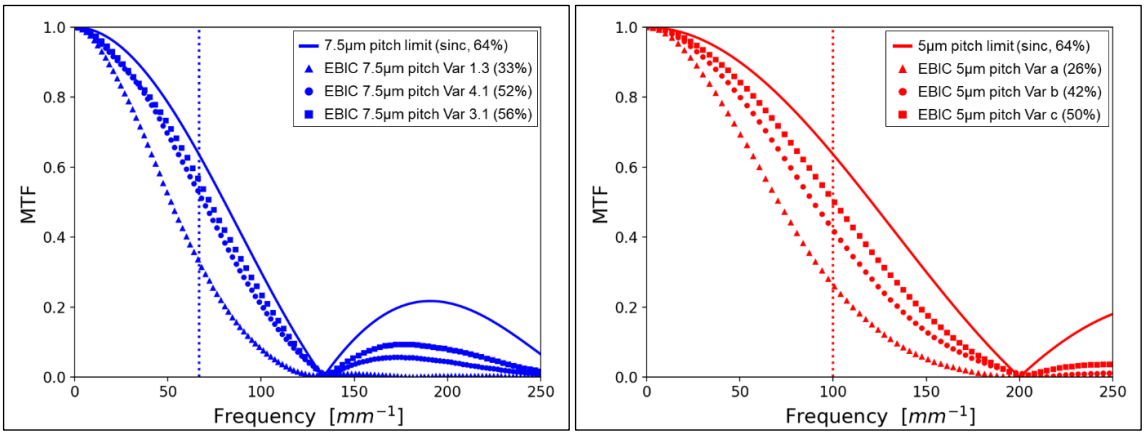

Figure 10. MTF measurements using EBIC setup in a SEM, 7.5µm on the left and 5µm on the right, MTF value are given at Nyquist frequency.

7. CONCLUSION

We demonstrate in this paper all the capabilities of the HOT NG p-on-n MWIR technology developed by CEA-LETI and Lynred. 7.5 µm pixel pitch have been characterized through superpixel VGA arrays (7.5 µm photodiodes coupled 4 by 4 to one ROIC pixel) and standard pixel SXGA arrays at 130K and above. Multiple diode design and technology process have been evaluated to determine the best configuration, by using subdivided arrays with different diode flavors. Photonic current and blackbody responsivity allowed determining a quantum efficiency of 85±5%, with high operability up to 99.98% and low dispersion (in the range 2-3%). Photodiodes RMS noise is shot-noise limited, with excellent operability, ranging from 99.99% on an array subzone to 99.97% on a full SXGA array at 130K. Some variant exhibits remarkable behavior while increasing the operating temperature up to 150K, with a very high operability and without any distribution tail increase. Diodes with RTN contribution have been studied on a couple of arrays on a long period (more than 30 minutes). It appears there is a strong correlation between the population of RMS noise and RTN defects. However, the number of RTN affected pixels is relatively low, comparable to the number of noise defective pixels. The number of RTN defects tends to increase with operating temperature, but this effect has still to be confirmed on other arrays. Finally, 5 µm pixel pitch diodes manufactured with the same technology have been presented. They behave very similarly to 7.5 µm diodes, with long bias plateau, but we need to get more statistical information to explore fully all the performances of this design. A proper combination of superpixel diodes and an adapted ROIC has yet to be done for such an evaluation. The MTF measurements of both 7.5 and 5 µm pixel pitch highlight the very good performances of the technology, with respectively 56% and 50% at Nyquist frequency.

ACKNOWLEDGEMENTS

This work was performed through DEFIR (Common Lab Lynred/CEA-LETI), with DGA (French MoD) funding.

REFERENCES

[1] Mollard et al, “Planar p-on-n HgCdTe FPAs by Arsenic Ion Implantation”, JEM 38(8), 1805–1813 (2009).

[2] Reibel et al, “MCT (HgCdTe) IR detectors: latest developments in France”, Proc. SPIE 7834, 78340M (2010).
[3] Rubaldo et al, “State of the art HOT performances for Sofradir II-VI extrinsic technologies”, Proc. SPIE Vol. 9819, 98191I (2016).
[4] Kerlain et al, “Mid-Wave HgCdTe FPA Based on P on N Technology: HOT Recent Developments. NETD: Dark Current and 1/f Noise Considerations”, JEM 45, 4557–4562 (2016).
[5] Gravrand et al, “HgCdTe Detectors for Space and Science Imaging: General Issues and Latest Achievements”, JEM 45, 4532–4541 (2016).
[6] Cervera et al, “Ultra-Low Dark Current HgCdTe Detector in SWIR for Space Applications”, JEM 46, 6142–6149 (2017).
[7] Pichon et al, “Asteroid and ALFA programs: to equip Europe with high performance IR detectors for space applications”, Proc. SPIE Vol. 12191, 121911N (2022).
[8] Baier et al, “Latest Developments in Long-Wavelength and Very-Long-Wavelength Infrared Detection with p-on-n HgCdTe” JEM 44, 3144–3150 (2015).
[9] Baier et al, “HgCdTe Diode Dark Current Modeling: Rule 07 Revisited for LW and VLW”, JEM 48, 5233–5240 (2019).
[10] Driggers et al, “Infrared detector size: how low should you go?”, Optical Engineering 51(6), 063202 (2012).
[11] Espuno et al, “A new generation of small pixel pitch/SWaP cooled infrared detectors”, Proc. SPIE Vol. 9648, 96480H (2015).
[12] S. Bisotto et al, “7.5µm and 5µm pitch IRFPA developments in MWIR at CEA-LETI”, Proc. SPIE Vol. 11002, 110021C (2019).
[13] .Gravrand et al, “Design of a small pitch (7.5µm) MWIR MCT array operating at high temperature (130K) with high imaging performances”, Proc. of SPIE Vol. 12107, 121070U (2022).
[14] Rubaldo et al, “Sub-10µm pitch HOT Technologies development at LYNRED”, Proc. SPIE, *to be published.*
[15] Hansen et al, “Energy gap versus alloy composition and temperature in $Hg_{1-x}Cd_xTe$”, JAP 53, 7099 (1982).
[16] S. Machlup, “Noise in Semiconductors: Spectrum of a Two-Parameter Random Signal”, JAP Vol. 25, pp. 341-343 (1954).
[17] Brunner et al, “Improvement of RTS Noise in HgCdTe MWIR Detectors”, JEM Vol. 43 no. 8, p. 3060-3064 (2014).
[18] Bustillos Vasco et al, “Use of EBIC for MTF measurements of HOT MCT focal plane planar array with very small pixel pitches”, Proc. SPIE, *to be published.*
[19] LeGoff et al, “Discussion on diffusion current suppression in HgCdTe MWIR detectors”, Proc. SPIE, *to be published.*
[20] Yèche et al, “Development of Electron Beam Induced Current Characterization of HgCdTe Based Photodiodes”, JEM 48, 6045–6052 (2019).
[21] Bustillos et al, “Modulation Transfer Function measurements by Electron Beam Induced Current of HgCdTe planar diode with small pixel pitch and high operating temperature”, JEM, *to be published*.